Journal of Solid State Chemistry **168,** 547–562 (2002)
doi:10.1006/jssc.2002.9752

Conducting Molecular Magnets Based on TTF-Derivatives

A. Miyazaki,*[,1] K. Enomoto,* K. Okabe,* H. Yamazaki,* J. Nishijo,* T. Enoki,* E. Ogura,† K. Ugawa,† Y. Kuwatani,† and M. Iyoda†

*Department of Chemistry, Tokyo Institute of Technology, 2-12-1 O-okayama, Meguro-ku, Tokyo 152–8551, Japan; †Department of Chemistry, Tokyo Metropolitan University, 1-1 Minami-Ohsawa, Hachioji, Tokyo 192-0397, Japan

Received January 8, 2002; in revised form May 10, 2002; accepted May 14, 2002

The crystal structures, electronic and magnetic properties of conducting molecular magnets developed in our group are reviewed. $(DMET)_2FeBr_4$ is composed of alternating stacks of quasi-one-dimensional (1D) donor sheets and square lattice magnetic anion sheets. This salt undergoes an SDW transition of the donor layer at 40 K and an antiferromagnetic transition of Fe^{3+} spins on the anion layer at 3.7 K. The one-to-one correspondence of the anomalies appearing on the magnetization curves with those on the magnetoresistance supports the presence of the π–d interaction. $(EDO–TTFI_2)_2[M(mnt)_2]$ (M = Ni,Pt) consists of 1D chains of conducting donors and magnetic anions aligned in parallel. These salts show metallic conductivity accompanied with a metal–insulator transition around 90 K. Localized spins on the anions behave as a 1D ferromagnet, whose origin is explained by McConnell's first model. The properties of related materials, $(EDTDM)_2FeBr_4$, $(EDS–TTF)_2FeBr_4$ and $(EDO–TTFBr_2)_2FeBr_4$, are also presented.

Key Words: **molecular conductors; molecule-based magnets; TTF derivatives; π–d interaction.**

1. INTRODUCTION

Physical properties of molecular metals and superconductors are one of the central interests in the field of solid-state physics and chemistry (1,2). From the discovery of charge-transfer complex TTF–TCNQ in 1973 (3), most of the molecular conductors are built with TTF-derivative molecules. The characteristic features of molecular conductors, in contrast to inorganic atom-based materials, can be summarized as follows. First, since the constituent molecules are planar in general and their HOMOs have π-orbital characters, the molecular conductors have inherent low-dimensionality in their electronic nature. As a result, these materials produce a large variety of physical phenomena characteristic of this low-dimensionality, such as Peierls transition, charge-density wave (CDW) or spin-density wave (SDW) states (4), Tomonaga–Luttinger liquid state (5), etc. Second, the TTF-moiety itself has a possibility of producing various derivatives by introducing substituents and/or exchanging chalcogen atoms, hence synthetic chemists can also contribute to enlarge the field of the novel electronic system. For example, when the parent molecule TTF is modified with two ethylenedithio groups, the resulting BEDT–TTF produces a number of molecular metals and superconductors (1). Due to these characteristics, TTF-based molecular conductors have fascinated both physicists and chemists.

Besides the electronic properties, magnetism is another important aspect of properties in solid-state science. Magnetic materials based on organic molecules are not only challenging targets for synthetic chemists, but also important for physicists especially from the viewpoints of low-dimensional quantum-spin system. However, although the electrical properties of solid-state organic materials have almost a half-century long history, the study of magnetic organic molecular materials has been lagging behind. One of the difficulties comes from the fact that the organic radicals with unpaired spins are in general kinetically unstable and easily form chemical bonds with neighboring molecules to annihilate the unpaired spins. In order to achieve their kinetic stability, the introduction of bulky protecting group around the radical center is necessary. However, this modification at the same time weakens intermolecular magnetic interaction between the organic radicals. For example, the first pure-organic ferromagnet, *p*-nitrophenyl nitronyl nitroxide (6) has the magnetic transition temperature of 0.60 K, which temperature is achieved only with ^{3}He refrigerator. As a matter of fact, this weakness of magnetic interaction does not hold for transition metal complexes with unpaired spins. Since the transition metal ions have partially filled *d*-orbitals, the

[1] To whom correspondence should be addressed. Fax: +81-3-5734-2242. E-mail: miyazaki@chem.titech.ac.jp.

0022-4596/02 $35.00

resulting complex molecules have localized spins without losing chemical stability. For example, decamethylferrocenium tetracyanoethlene $[Fe(C_5Me_5)_2]TCNE$ undergoes a ferromagnetic transition at 4.8 K (7), which temperature is reached using a simple liquid ^4He cryostat.

The hybridization of molecular metals and magnetic transition metal complexes gives an important feature to the physics and chemistry. When magnetic ions with *d*-electrons are introduced as a counterpart for organic donors in charge-transfer complexes, an exchange interaction defined as a π–*d* exchange interaction will be present between the donors and anions. In this case, π-conduction carriers work to mediate the exchange interaction between the localized magnetic moments of *d*-electrons. This system is regarded as the molecular version of the ordinary inorganic metallic magnetic system with transition metal, where the exchange interactions between the spins are achieved through the *s*–*d* or *s*–*f* interaction. Even when the organic metallic systems occasionally have insulating ground states, due to the instability inherent to the low-dimensionality (Peierls instability, charge-density wave), or strong correlation between the π-electrons (Mott insulator, spin-density wave), π-electrons can be coupled with the magnetic moments of *d*-electrons through the π–*d* exchange interaction to produce novel magnetic systems. Based on these viewpoints, we have developed a number of molecular magnets based on TTF-type derivatives, and investigated their electronic and magnetic properties in detail (8). For example, $(BEDT–TTF)_3CuBr_4$ undergoes an antiferromagnetic transition at $T_N = 7.65$ K, where the large exchange interaction between the magnetic $CuBr_4^{2-}$ anions ($J = -15.7$ K) is explained in terms of the cooperation of the extended nature of the unpaired *d*-electrons of $CuBr_4^{2-}$ anions and the close intermolecular donor–anion contacts (9). A molecular weak ferromagnet ($C_1TET–TTF)FeBr_4$ is featured as a triangle-based ladder magnetic system, where the superexchange interaction between the *d*-electron spins on magnetic anions is mediated by the π-electrons system of the donor molecules (10). Such π–*d* interaction-based conducting molecular magnets also attract many research groups to extend the fields of the molecule-based magnets (11). One of the pioneering works among them which is still regarded as a representative material in this field is λ-$(BETS)_2MCl_4$ (M = Fe, Ga) (12). The $FeCl_4$ salt shows a π–*d* coupled antiferromagnetic state including the field-induced superconductivity (13).

The present article extends our recent work on the physical properties of conducting molecular magnets based on TTF-type organic donors such as DMET, EDTDM, EDS–TTF and EDO–TTFX_2 (X = I, Br) presented in Fig. 1, with counter anions having localized moments of *d*-electrons. In the next section, we will discuss our strategy for obtaining conducting molecular magnets. In Section 3, the discussion is devoted to the salt $DMET_2FeBr_4$, in which the presence of the π–*d* exchange interaction is directly proved by the comparison of its transport and magnetic properties. The magnitude of the π–*d* exchange interaction is systematically investigated by the chalcogen substitution of the donor part by using EDTDM and EDS–TTF, whose results are also discussed. In Section 4 we discuss the molecular conducting magnets based on EDO–TTFX_2. This molecule also produces π–*d* interaction-based molecular magnet with the $FeBr_4$ anion, where the intermolecular halogen$\cdots$halogen interaction plays an important role in regulating the crystal structure and transmitting the magnetic interaction. The salts of this donor with $M(mnt)_2$ anions (M = Ni, Pt; mnt = maleonitriledithiolate) are also presented, which are first examples of molecular conductor with magnetic anions which shows metallic conduction and ferromagnetic interaction simultaneously.

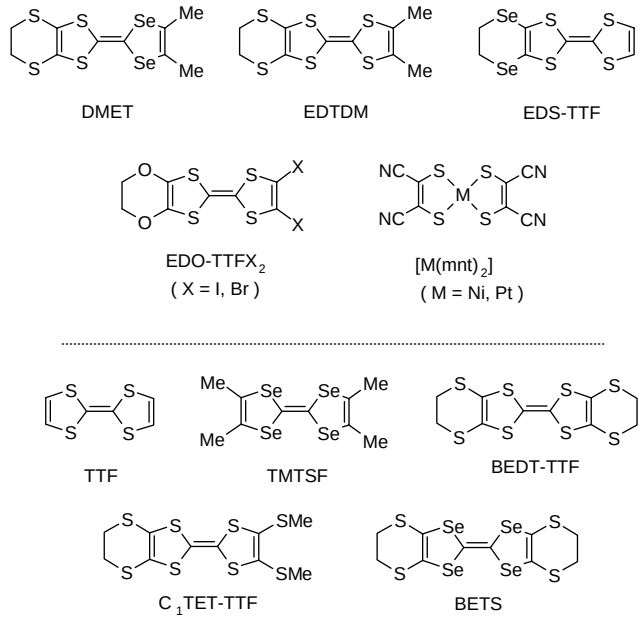

FIG. 1. Molecular structures of donor molecules; DMET (4,5-ethylenedithio-4′, 5′-dimethyl-1,3-dithia-1′,3′-diselenafulvalene), EDTDM (4,5-ethylenedithio-4′,5′-dimethyltetrathiafulvalene), EDS–TTF (4,5-ethylenediselenotetrathiafulvalene), EDO–TTFX_2 (X = Br, I; 4,5-ethylenedithio-4′,5′-dihalotetrathiafulvalene), $M(mnt)_2$ (M = Ni, Pt; mnt = malononitriledithiolate), TTF (tetrathiafulvalene), TMTSF (tetramethyltetraselenafulvalene), BEDT–TTF (bis(ethylenedithio)tetrathiafulvalene), C_1TET–TTF (4,5-ethylenedithio-4′,5′- bis(methylthio)tetrathiafulvalene), and BETS (bis(ethylenedithio)tetraselenafulvalene).

2. APPROACH TO CONDUCTING MOLECULAR MAGNETS

Here we describe our strategy for achieving conducting molecular magnets based on the π–*d* exchange interaction

in TTF-type salts with transition metal complexes, where TTF donors based on π-electrons and magnetic anions having localized spins of d-electrons contribute to electron transport and magnetism, respectively. Before doing this, we first summarize the discussion on the electronic structure of the pure TTF-based organic conductors in terms of the Hubbard Hamiltonian, because it can give some suggestions to designing π–d interaction system as we will see later. In the TTF-based organic conductors, the constituent donor molecules are in a partially oxidized state, and the transport carriers (electrons or holes, depending on the degree of the oxidation) of the conductors belong to the highest occupied molecular orbitals (HOMOs) of the constituent donor molecules. The movement of the carriers in a solid can be described using two fundamental parameters, the transfer integral t and the on-site Coulomb repulsion energy U. The transfer integral t is given by the following equation:

$$t = \int \psi_i^*(\mathbf{r})\hat{H}\psi_{i+1}(\mathbf{r})\, d\mathbf{r}, \qquad [1]$$

where $\hat{H}$ is the Hamiltonian for the one electron term, and $\psi_i(\mathbf{r})$ is the wave function of the HOMO of the ith donor molecule. This transfer integral t is interpreted as an intermolecular version of resonance integral β appearing in the Hückel molecular orbital theory. From the viewpoint of molecular design, this quantity can be controlled by suitable introduction of substituents and/or chalcogen substitution, such as the modifications of TTF into BEDT–TTF and TMTSF (Fig. 1). On the other hand, the on-site Coulomb repulsion energy U is defined as

$$U = E(2) + E(0) - 2E(1), \qquad [2]$$

where $E(n)$ is the energy of a donor molecule whose HOMO contains n electrons. Obviously, the quantity U vanishes under the one-electron approximation scheme where the relation $E(2) - E(0) = 2(E(1) - E(0))$ holds, since electrostatic repulsion between two electrons on the same molecule is neglected for this case. Therefore, U can be understood in terms of the electrostatic potential

$$U \approx e^2/\varepsilon r, \qquad [3]$$

where ε is the dielectric constant and r is the mean distance between two electrons in the HOMO of the molecule, which corresponds to the size of the π-electron system on the molecule itself. For example, the on-site Coulomb repulsion can be reduced by the extension of the molecular π-orbital, such as the introduction of the electron-rich substituents into the parent TTF moiety.

Using these parameters, the electronic state of molecular conductors is described with the Hubbard Hamiltonian

$$\hat{H} = U\sum_i n_{i\uparrow}n_{i\downarrow} + t\sum_{i,\sigma}\left(c_{i,\sigma}^+ c_{i-1,\sigma} + c_{i-1,\sigma}^+ c_{i,\sigma}\right), \qquad [4]$$

where $c_{i,\sigma}^+$ and $c_{i,\sigma}$ are the creation and annihilation operators, respectively, for the electron on the ith molecule having σ ($=\uparrow$ or $\downarrow$) spin, and $n_{i,\sigma} \equiv c_{i,\sigma}^+ c_{i,\sigma}$ is the number operator for this electron. The second term of the Hamiltonian describes the kinetic energy for the movement that an electron jumps from molecule $i-1$ to molecule i and vice versa. Since t is negative, this movement energetically stabilizes the electronic system. On the other hand, the first term appears only if two electrons are present on the same molecule, hence it suppresses the intermolecular motion of the electrons. This competition between these two terms produces a large variety of electronic structures in molecular systems. The condition $t \gg U$ favors itinerant metallic states, whereas the condition $t \ll U$ stabilizes localized insulating states. In the latter case, the Hubbard Hamiltonian is reduced to the Heisenberg Hamiltonian

$$\hat{H} = -J\sum_i \boldsymbol{S}_i \cdot \boldsymbol{S}_{i+1}, \qquad [5]$$

where J is the exchange interaction, and $\boldsymbol{S}_i$ is the spin operator for the electron located on the ith molecule. By directly solving the Hubbard Hamiltonian for two-molecule system having two electrons, J is expressed with U and t as

$$J = -\frac{4t^2}{U} \qquad [6]$$

under the condition of $t \ll U$.

Similar discussion is also applicable to the interaction between the π-electrons on the donor layer and the d-electrons on the magnetic anion layer. The Hubbard Hamiltonian for a donor–anion pair is expressed as

$$\hat{H} = U_\pi n_{\pi\uparrow}n_{\pi\downarrow} + U_d n_{d\uparrow}n_{d\downarrow} + t_{\pi d}\sum_\sigma \left(c_{\pi\sigma}^+ c_{d\sigma} + c_{d\sigma}^+ c_{\pi\sigma}\right), \qquad [7]$$

where suffixes π and d denote the π- and d-electron systems, respectively, and $t_{\pi d}$ is the transfer integral between them. Solving this Hamiltonian, the magnitude of the π–d exchange interaction is evaluated as

$$J = -2t_{\pi d}^2\left(\frac{1}{U_\pi} + \frac{1}{U_d}\right). \qquad [8]$$

This result shows the guideline for achieving large π–d exchange interaction between the donor and anion systems, i.e., the decrease of the on-site Coulomb repulsions for donor and anion molecules, and the increase of the transfer integral between them. We can therefore select the

constituent transition metal complex anion and TTF-type donor molecules in the following way. When the unpaired *d*-electrons of the central metal for the anion are delocalized to the ligands, the on-site Coulomb repulsion for the anion U_d is reduced. At the same time, this delocalization increases the spin density on the ligands that are located close to the donor counterparts, and intermolecular transfer integral $t_{\pi d}$ increases simultaneously. From these points magnetic anions such as MBr_4^{n-} or $[M(S_2C_2R_2)_2]^{n-}$ ($M = 3d$ transition metal; $R = CN$, etc.) are plausible, since their central metals (M) and ligands (Br^-or $S_2C_2R_2^{2-}$) are connected not only with σ-bonding but also with π-bonding, which enables the back donation of the unpaired *d*-electrons from the central metal to the ligands. For the donor part, the reduction of U_π and increase of $t_{\pi d}$ are required for obtaining metallic systems as we have already discussed before. Therefore, our strategy for the design of conducting molecular magnet is summarized as the combination of highly polarizable magnetic anion with donor molecules that are guaranteed to give good metallic systems.

3. $(DMET)_2FEBR_4$ AND RELATED SALTS

3.1. $(DMET)_2FeBr_4$

DMET is an asymmetric donor regarded as a hybrid of TMTSF and BEDT–TTF (Fig. 1). The first aim in designing this molecule was to extend the world of molecular conductors by reproducing the characteristics of these two donors (1). TMTSF molecule has a strong tendency of quasi-1D stable metals regardless of counter anions, including the first organic superconductor $TMTSF_2PF_6$ (14). On the other hand, the crystal structures of BEDT–TTF salts show a large variety of donor packing patterns which are categorized as α-, β-, θ- and κ-type structures (15). According to these structural motifs, their physical properties have a large variety extending from insulators, metals to superconductors (1).

DMET molecule forms salts with various counter anions in a 2:1 stoichiometry (16). Since the TMTSF part and BEDT–TTF part of this molecule have different thickness due to the difference in the van der Waals radii of sulfur (1.80 Å) and selenium (1.90 Å) (17), this donor molecule has a strong tendency of forming 1D column with head-to-tail overlapping modes with large intermolecular transfer integrals. The physical properties of $(DMET)_2X$ salts depend on the molecular shape of the counter anion. The salts with octahedral anions (PF_6^- and AsF_6^-) show semiconductive behavior. For the tetrahedral anions (BF_4^- and ClO_4^-), on the other hand, the electrical conductivity reveals the metallic behavior down to ca. 40 K where metal–insulator transition takes place, and the insulator phase is characterized as an SDW state (18). When the counter anion is a linear anion, such as I_3^-, IBr_2^- or AuX_2^- ($X = I$, Br, Cl, CN), the salt shows metallic properties and undergoes a superconducting transition, whose transition temperature depends on the size of the counter anion (16). Due to this high ability of DMET donor in forming a stable metallic system, we have focused on this donor molecule as the constituent of the organic part of the π–*d* interaction-based molecular magnets (19).

Figure 2 shows the crystal structure of $(DMET)_2FeBr_4$. The donor molecules are stacked to form uniform 1D columns. The column located at $z \sim 0$ and $1/2$ are extended along the $a+b$ and $a-b$ directions, respectively. This difference in the column elongation directions, which can be referred to as the "double-column" structure, is observed also in the crystal of $(DMET)_2BF_4$ (20). However, the detailed stacking mode of the donor molecules is somewhat different between these salts. Comparison of the transfer integrals calculated using the extended Hückel Hamiltonian (21) shows that the $FeBr_4$ salt has almost uniform donor columns, whereas for the BF_4 salt the donor columns are dimerized. The uniform donor columns then interact with each other through close Se···S intermolecular contacts (distance: 3.72 Å) to form a sheet structure on the *ab*-plane. However, the strength of the interchain interactions (0.06–0.1 eV) is 10–20% of the intrachain ones, hence this salt is regarded as a quasi-1D system. The calculated band structure of this salt suggests a $\frac{3}{4}$ filled 1D metallic state. Because of the "double column" structure, the Fermi surfaces for the columns around $z \sim 0$ and $\frac{1}{2}$ are independent and are extended to the different directions. Due to this "multi Fermi surfaces" feature, which explains the stability of 1D metallic states in β-$Me_4N[M(dmit)_2]_2$ ($M = Ni$, Pd) (22), this $FeBr_4$ salt is expected to have a stable metallic system, or at least the Peierls distortion can be suppressed. The tetrahedral $FeBr_4^-$ anions form a distorted square lattice formed by Br···Br contacts, whose distance (3.88 Å) is slightly longer than twice that of the van der Waals distance of the bromine atom ($2 \times 1.85 = 3.70$ Å) (17). These anion sheets then interact with the donor sheets through intermolecular Br···S contacts, whose distance (3.76 Å) is comparable to the corresponding van der Waals distance (3.65 Å). Therefore, the structure of this salt is characterized with the alternating stacking of DMET donor conducting sheets and $FeBr_4^-$ magnetic sheets, between which interlayer interactions with considerable strengths are expected. $(DMET)_2GaBr_4$, the salt with diamagnetic counter anion, is isomorphous to $(DMET)_2FeBr_4$, hence this $GaBr_4$ salt can be treated as a reference material to estimate the effect of π–*d* interaction of the $FeBr_4$ salt.

Figure 3 presents the temperature dependence of the electrical resistivity for $(DMET)_2FeBr_4$ and $(DMET)_2GaBr_4$. The conductivity of the $FeBr_4$ salt at room temperature is 15 S cm^{-1}, which is comparable to the other

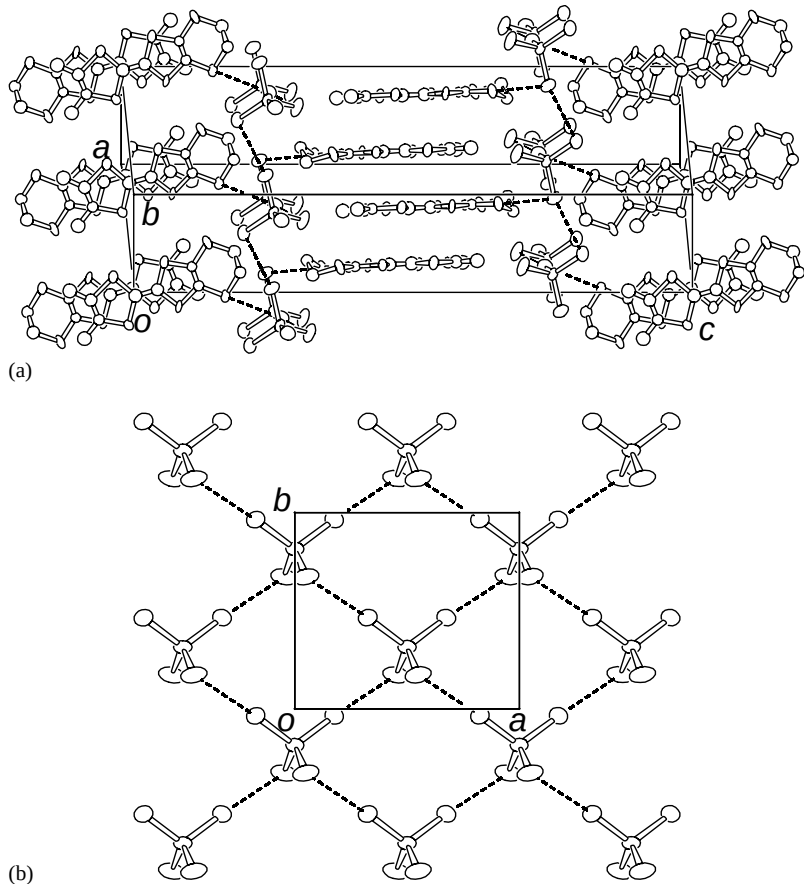

FIG. 2. (a) Crystal structure of $(DMET)_2FeBr_4$ projected on the $[1\bar{1}0]$ plane. (b) Structure of the quasi-square-lattice anion sheet. Dashed lines in both the figures denote close intermolecular Br···Br and Br···S contacts.

metallic DMET salts (16). From the peak appeared in the T vs $d\ln\rho/d(T^{-1})$ plot (inset of Fig. 3), the metal–insulator transition temperature is estimated at $T_{MI} \sim 40$ K regardless of the counter anion, which is close to that of the BF_4 salt (23). This metal–insulator transition is also confirmed from the static susceptibility of $DMET_2GaBr_4$, where the susceptibility comes only from the π-electron part. Above T_{MI}, the susceptibility shows small temperature dependence ascribed to the Pauli paramagnetism, whereas below T_{MI} it shows steep decrease showing the disappearance of the conduction electrons. This result therefore shows that the metal–insulator transition cannot be assigned to the Mott transition. If we take into consideration the fact that X-ray oscillation photograph shows no difference between above and below T_{MI}, the possibility of CDW transition can also be ruled out. Therefore, the nature of this metal–insulator transition can be presumably assigned to the SDW transition.

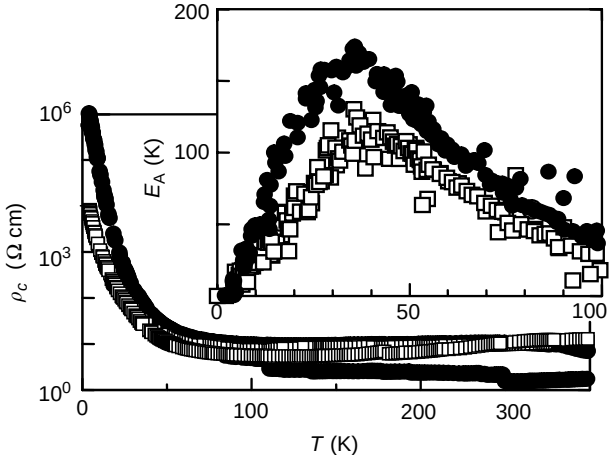

FIG. 3. Temperature dependence of the resistivity of $(DMET)_2FeBr_4$ (open squares) and $(DMET)_2GaBr_4$ (filled circles). Inset: temperature dependence of the activation energies.

The magnetic susceptibility obeys the Curie–Weiss law in the high-temperature regime (Fig. 4(a)). The Curie constant C and the Weiss temperature Θ are estimated at 4.4 emu K mol^{-1} and -5.7 K, respectively. This Curie constant C is in good agreement with the calculated value of the $S = 5/2$ magnetic anion contribution. This salt undergoes an antiferromagnetic transition at $T_N = 3.7$ K. Since no short-range order hump is observed in the susceptibility above T_N, this salt can be treated as a

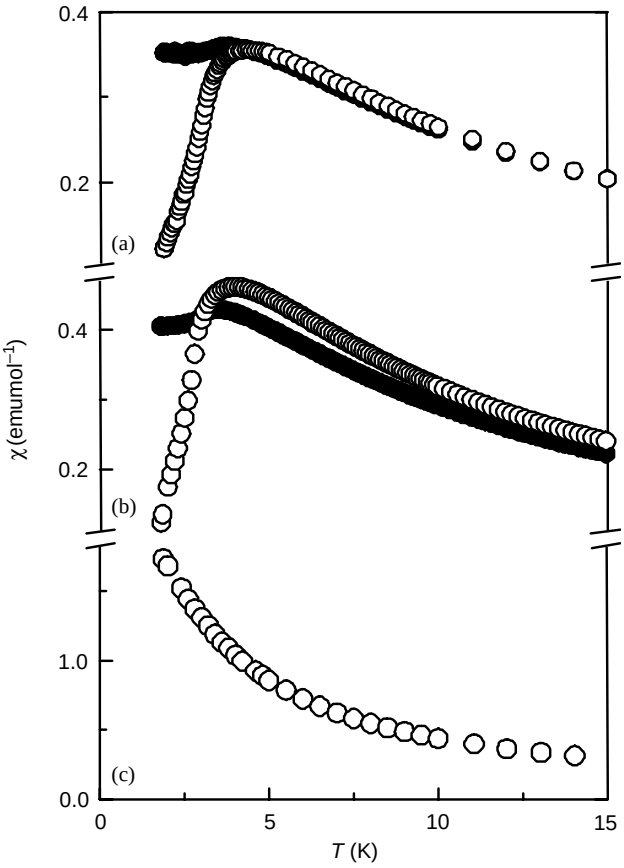

FIG. 4. Temperature dependence of the magnetic susceptibility of (a) $(DMET)_2FeBr_4$, (b) $(EDTDM)_2FeBr_4$, and (c) $(EDS\text{-}TTF)_2FeBr_4$, in a field of 1 T. Open circles: $B \parallel a$-axis, filled circles: $B \parallel b$-axis.

three-dimensional (3D) magnetic system, where donor π-electrons bridging anion quasi-square lattice produce interlayer exchange paths. The magnetization curve at 1.8 K (Fig. 5) shows a spin–flop transition at $B_{SF} = 2$ T when the external field is applied parallel to the spin easy axis ($= a$-axis). It should be noted that the easy-axis magnetization curve is beyond the hard-axis magnetization curve above the spin–flop field B_{SF}, and has a shoulder around $B_1 = 3.5$ T. Similar shoulder is observed also for the hard-axis ($= b$-axis) magnetization curve around $B_2 = 5$ T. These anomalies more clearly appear as peaks on the dM/dB vs B curves, i.e., field dependence of the magnetic susceptibilities (Fig. 5). These unusual magnetic behavior cannot be explained in terms of Fe^{3+} ($S = 5/2$) spins alone, strongly suggesting that the donor molecules effectively participate in the magnetic behaviors.

For the purpose of confirming the contribution of the donor π-electron system in the magnetism, the magnetoresistance is measured on applying the external field along the a- and b-axis. Figure 6 presents the field dependence of the magnetoresistance measured at 1.6 K ($< T_N$). For the in-plane transport ($\rho\parallel$), the negative magnetoresistance is observed up to 15 T with a minimum appearing around 6 T. At the external field corresponding to B_{SF}, an anomalous discontinuity is detected for the easy axis direction. In contrast, the interplane magnetoresistance ($\rho_\perp$) is negative only up to ca. 5 T with a spin–flop-induced singularity in the easy axis direction, while the magnetoresistance becomes positive above that field. For the hard axis direction, the magnetoresistance is positive with a discontinuous change at $B_2 = 5$ T, at which the magnetization has an anomaly. This one-to-one correspondence between the magnetoresistance and magnetization is a direct evidence for the presence of the π-d interaction.

The origin of the correlation between the transport and magnetic behavior can be understood as follows. Below T_{MI}, the donor system is in the SDW state, and localized spins generated are spatially ordered with a four-fold periodicity. Below T_N, the anion spins become antiferromagnetically ordered with a two-fold periodicity. The localized donor spins are then coupled with the anion spins to gain stabilization energy, hence the translational motion of SDW that causes the transport in the insulator phase destabilizes the magnetic energy. When the applied field becomes strong enough to arrange all anion spins ferromagnetically, no energy is required in the SDW translational motion. Therefore, the elevation of the field

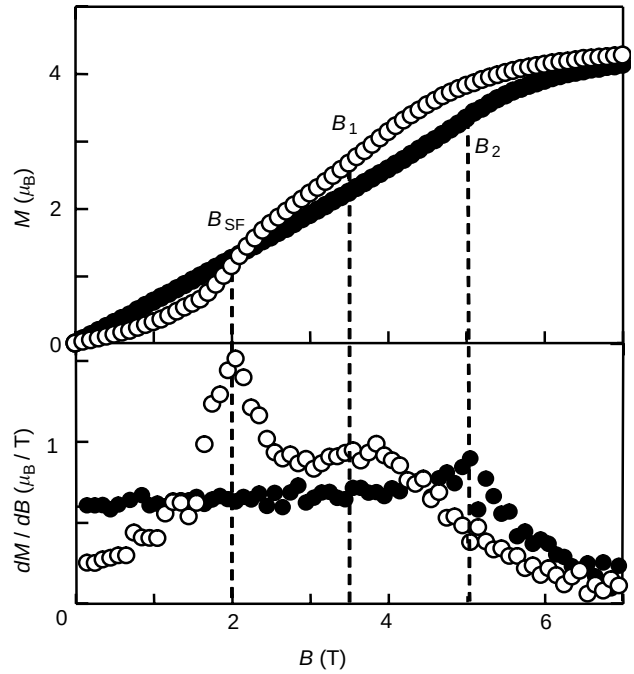

FIG. 5. Magnetization curves of $(DMET)_2FeBr_4$ at 1.8 K. Open circles: $B \parallel a$-axis, filled circles: $B \parallel b$-axis. Magnetic susceptibilities (dM/dB) are also plotted as a function of the field. B_{SF} denotes the spin–flop transition and B_1, B_2 show anomalies on the magnetization curves (see text).

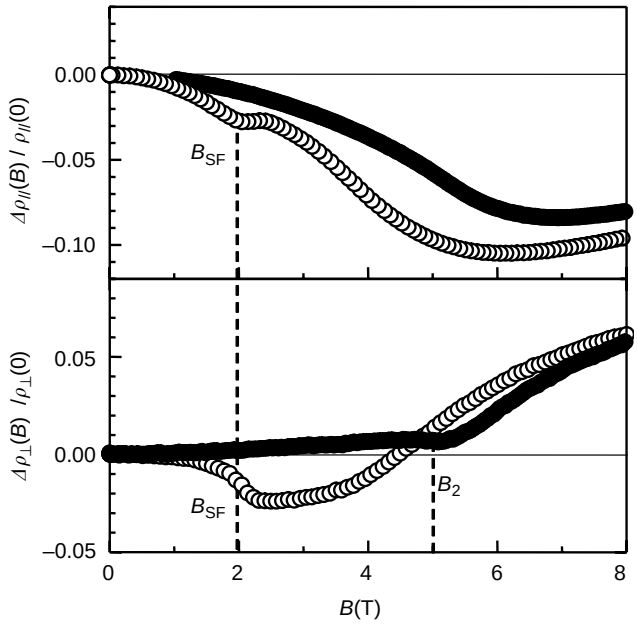

FIG. 6. Field dependence of the magnetoresistance of $(DMET)_2FeBr_4$ measured at 1.6 K for the in-plane ($\Delta\rho_{\parallel}(B)/\rho_{\parallel}(0)$) and out-of-plane ($\Delta\rho_{\perp}(B)$ / $\rho_{\perp}(0)$) directions. Open circles: $B \parallel a$-axis, filled circles: $B \parallel b$-axis. The fields corresponding to the spin–flop transition (B_{SF}) and the anomaly (B_2) appearing on the magnetization curve are also indicated.

gives negative magnetoresistance up to the saturation field of Fe^{3+} spins. The anomaly at B_{SF} in the magnetoresistance is the consequence of a change in the magnetic energy accompanied with the spin–flop transition, which modifies the ease in the SDW translational motion.

3.2. $(EDTDM)_2FeBr_4$

If the donor molecules of $(DMET)_2FeBr_4$ can be substituted with analogues keeping the crystal structure unchanged, it is possible to investigate systematically the role of the π-electron system in the π–d interaction-based molecular magnets. Based on this viewpoint, we prepared $(EDTDM)_2FeBr_4$, all-sulfur version of $(DMET)_2FeBr_4$, to compare their physical properties with $(DMET)_2FeBr_4$ (24).

The crystal structures of the two salts $(EDTDM)_2FeBr_4$ and $(EDTDM)_2GaBr_4$ are close to that of $(DMET)_2FeBr_4$ (Fig. 2). Namely, the donor molecules form the "double-column" structure and the $FeBr_4^-$ anions form quasi-square-lattice two-dimensional (2D) magnetic sheets. However, from the comparison of intermolecular overlap integrals between $(EDTDM)_2FeBr_4$ and $(DMET)_2FeBr_4$, the donor columns of the EDTDM salt are slightly dimerized and have weaker side-by-side interactions between donors compared to the DMET salt. The distances of the intermolecular Br···Br contacts between anions (3.87 Å) and Br···S contact between anion and donor (3.74 Å) are similar to the corresponding values of the DMET salt. Since the structural difference between the EDTDM salt and DMET salt is concentrated on the donor site, we can expect that the comparison of their physical properties reveals the role of the π-electrons in the π–d interaction systems.

For both $(EDTDM)_2FeBr_4$ and $(EDTDM)_2GaBr_4$, the in-plane resistivity shows metallic behavior above ca. 200 K and semiconducting behavior below 200 K. However, the magnetic susceptibility of $(EDTDM)_2GaBr_4$ shows Pauli paramagnetic behavior above 20 K, whose contribution gradually decreases as the temperature is lowered. Since the Pauli paramagnetic susceptibility is proportional to the density of states at the Fermi level, the decrease in the carrier concentration explains the apparent semiconductor-like behavior in the resistivity for $T<200$ K even in the metallic phase. Below 20 K, the susceptibility steeply decreases as the temperature decreases, suggesting the appearance of an antiferromagnetic ordered state. According to the recent ^{13}C-NMR measurement for the ^{13}C-enriched sample by Miyagawa *et al.*, the spin–lattice relaxation rate T_1^{-1} takes a peak at ca. 15 K showing the presence of a magnetic transition, and a SDW state is suggested as a ground state.

The susceptibility obeys the Curie–Weiss law in the high-temperature region above 50 K, where the Curie constant C and the Weiss temperature Θ are estimated at 4.7 emu K mol^{-1} and –2.8 K, respectively (Fig. 5(b)). From the Curie constant, it is proved that Fe^{3+} high-spin species ($S=5/2$) mainly serves as the origin of the magnetism of $(EDTDM)_2FeBr_4$. This salt shows an antiferromagnetic transition at $T_N=3$ K, below which the magnetic easy axis is the a-axis. Figure 7 shows the magnetization curves at 1.9 K for $(EDTDM)_2FeBr_4$. From the magnetization curves, a spin–flop transition occurs at $B_{SF}=1.8$ T in addition to the appearance of an anomaly at $B_1=2.9$ T when the magnetic field is applied along the a-axis. When the field is parallel to the b-axis, the magnetization curve has a shoulder around $B_2=4.5$ T. The comparison of the magnetization curves with those of the DMET salt reveals that the spin–flop field B_{SF} is almost unchanged, while the anomalies at B_1 and B_2 appear at the lower field. Since the main differences between these two salts are in the π-electron part, it is suggested that the anomalies at B_1 and B_2 are related to the participation of the donor in the magnetism.

One of the virtues of the selenium-to-sulfur substitution is the ease of the ESR measurements, since for DMET salts the large spin–orbit coupling for the selenium atom broadens the line width of the ESR absorption. The ESR signal of $(EDTDM)_2GaBr_4$ appears as one Lorentzian peak with line width $\Delta H_{pp}=0.7$ mT and g-value $g=2.01$ at room temperature when the field is applied along

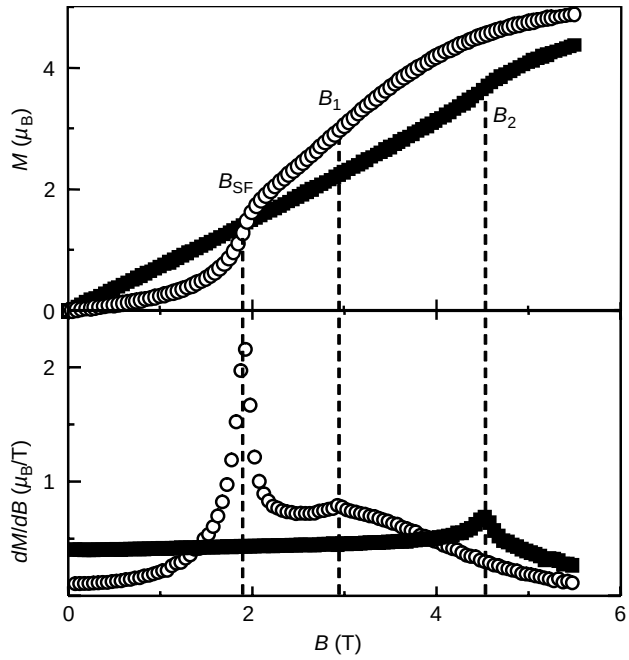

FIG. 7. Magnetization curves of $(EDTDM)_2FeBr_4$ at 1.9 K. Open circles: $B\|$ a-axis, filled circles: $B\|$ b-axis. Magnetic susceptibilities (dM/dB) are also plotted as a function of the field. B_{SF} is the spin–flop transition field and B_1, B_2 show anomalies on the magnetization curves (see text).

the out-of-plane direction ($=c$-axis). In contrast, in the applied field along the $a\pm b$ direction in the conduction plane, two Lorentzian peaks are observed with g-value $g=2.0079$ and 2.0025, which is the consequence of the "double-column" structure. Since the long axes of donor molecules are parallel to the c-axis, two donor columns are equivalent for this direction, giving a single absorption. On the other hand, when the field is applied in the conducting plane, two columns are generally non-equivalent, giving two peaks in the ESR spectra whose g-values correspond to the side-by-side direction and the normal of the molecular plane, respectively. For the $FeBr_4$ salt, a broad ESR signal ($\Delta H_{pp}=55$ mT) is detected, which is assigned to the localized spins on the $FeBr_4^-$ anions. This line width increases with decreasing temperature and below 15 K it abruptly diverges (Fig. 8(a)), which is consistent with the appearance of the SDW state below 15 K as previously described. Since there is a possibility for the $FeBr_4$ salt that the contribution of the π-electron spins is concealed by the large d-electron spins, the ESR spectra of the spin-diluted mixed salt $(EDTDM)_2Fe_{0.01}Ga_{0.99}Br_4$ is also investigated to elucidate the interaction between the π- and d-electrons. The ESR signal of the mixed salt appears as a single Lorentzian peak without separating the contribution of π- and d-electron spins regardless of the direction of the applied field. This coalescence shows the presence of the exchange interaction between the π- and d-electron spins, i.e., the neighboring two donor columns interact with each other via localized Fe^{3+} spins. The temperature dependence of the g-values (Fig. 8(b)) shows that the g-value of the mixed salt is shifted from that of the $GaBr_4$ salt, and the magnitude of this shift becomes larger as the temperature decreases. Due to the coalescence of the ESR absorptions from the π- and d-electron spins, the observed g-value is expressed as $g=(\chi_\pi g_\pi+\chi_d g_d)/(\chi_\pi+\chi_d)$, where g_π and g_d are the g-values and χ_π , χ_d are the spin susceptibilities of the π- and d-electron spins, respectively. The π-part χ_π has small temperature dependence because of the Pauli paramagnetism, whereas χ_d has a Curie-like behavior. The contribution of the d-electron spin therefore becomes larger as the temperature decreases, which leads to the downward g-value shift.

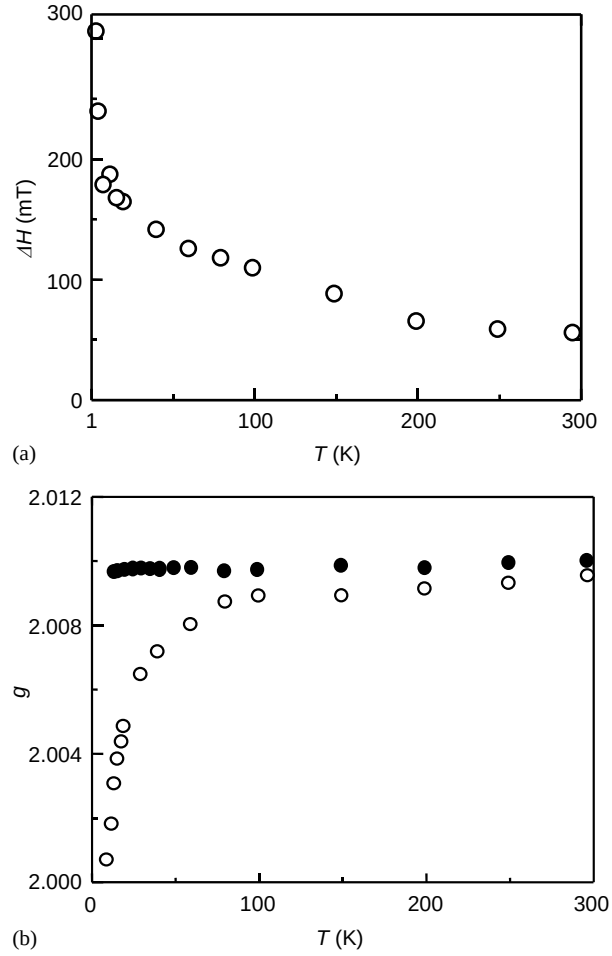

FIG. 8. (a) Temperature dependence of the ESR line width of $(EDTDM)_2FeBr_4$, with the external field applied parallel to the a-axis. (b) Temperature dependence of the ESR g-values of $(EDTDM)_2Fe_{0.01}Ga_{0.99}Br_4$ (filled circles) and $(EDTDM)_2GaBr_4$ (open circles).

The apparent semiconductive behavior of this salt is suppressed by applying the hydrostatic pressure to the sample. As the pressure increases, the temperature for the resistivity minimum decreases. When the applied pressure is around 0.92 GPa, the resistivity shows an anomaly around the Néel temperature T_N, which is clearly observed on the E_A (activation energy) vs T plot (Fig. 9). This anomaly gradually disappears by further application of the pressure. These results suggest that the magnetic ordering of the localized *d*-electrons strongly affects the conducting π-electrons, especially in this marginal pressure region between the SDW and metallic states. In the low-pressure regime ($P<0.5$ GPa), the conduction π-electrons are already localized at T_N due to the SDW generation, hence the antiferromagnetic transition of the anion layer does not work effectively on the π-electrons. In the high-pressure region ($P>1.35$ GPa), on the contrary, the metallic state is stabilized so that the effect of magnetic ordering of the anions is not strong enough to induce the transition. In the marginal region ($P\sim0.92$ GPa), the antiferromagnetic transition of the anion layer can lead to induce SDW transition of the π-electrons as a consequence of the π–d interaction between donors and anions. A preliminary experiment in this pressure region shows a giant negative magnetoresistance ($\Delta\rho(B)/\rho(0) = -0.6$ for $B>7$ T), also showing the high sensibility of the π-electron system of the donor layers to the magnetic ordering of the anion layers.

3.3. *(EDS–TTF)$_2$FeBr$_4$*

$(EDTDM)_2FeBr_4$ shows magnetic properties similar to $(DMET)_2FeBr_4$ in spite of different electron transport properties. This might come from the similarity of intermolecular Br···S contact, which is expected to be responsible for the realization of the π–d interaction. It is therefore expected that the modification of the π–d interaction can be achieved by the selenium substitution at the outer six-membered ring of the donor. Based on this viewpoint, crystal structure and physical properties of the novel molecular conductor $(EDS–TTF)_2FeBr_4$ were investigated.

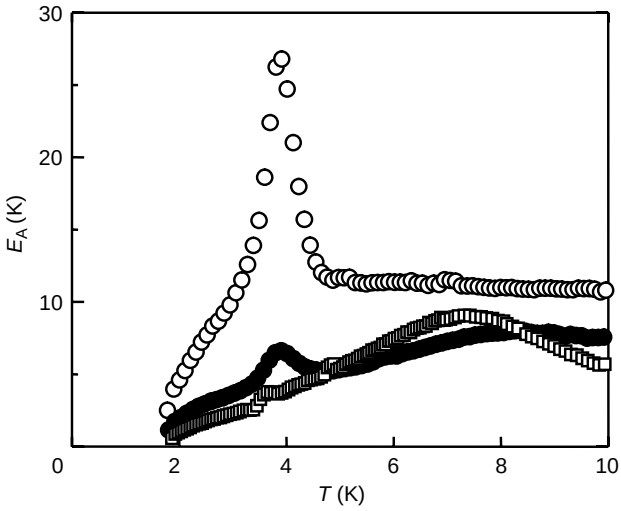

FIG. 9. Temperature dependence of the activation energy for the resistivity of $(EDTDM)_2FeBr_4$ under hydrostatic pressures. Open circles: $P=0.92$ GPa, filled circles: $P=1.35$ GPa, open squares: $P=1.76$ GPa.

The crystal structure of $(EDS–TTF)_2FeBr_4$ is similar to that of $(DMET)_2FeBr_4$ and $(EDTDM)_2FeBr_4$ (Fig. 2), in spite of the absence of two methyl groups in the donor molecule. A remarkable difference within the donor layer is the dimerization of the donor stacks. The ratio of intra- to interdimer transfer integrals within a donor column is estimated at 1.33, which is larger than the corresponding values for $(DMET)_2FeBr_4$ (1.02) and $(EDTDM)_2FeBr_4$ (1.12). The donors and anions are connected via close Br···Se contacts, whose distance (3.49 Å) is shorter than the sum of van der Waals radii of Br and Se (3.75 Å) (17). Between the 1,3-dithiol ring of the donor and bromide ligand of anion, CH···Br type hydrogen bond (C···Br: 3.55 Å) is also observed.

The salt shows high conductivity at room temperature ($400\ S\,cm^{-1}$) and metallic properties down to ca. 250 K. Below this temperature it behaves as a semiconductor with the activation energy $E_A=380$ K. The result of the band structure calculation shows that the EDS–TTF salt has stronger 1D character than the DMET and EDTDM salts. This one dimensionality and/or dimerization of the donor columns can be responsible for the metal–insulator transition.

The magnetic susceptibility obeys the Curie–Weiss law with the Curie constant $C=4.58$ emu K mol^{-1} and Weiss temperature $\Theta=-0.93$ K (Fig. 5(c)). Despite the presence of the close Br···Se contacts between the anion and donor layers, the exchange interaction between the magnetic anions is negligible, and no magnetic phase transition is observed down to 1.8 K. The magnetization curve at 2 K is well fitted with the Brillouin curve for $S=5/2$ spins, showing little exchange interaction between the localized spins on the anions.

The semiempirical molecular orbital calculation using PM3 Hamiltonian (25) reveals that the Se 4*p* orbital hardly contributes to the HOMO of the EDS–TTF molecule (atomic orbital coefficient = 0.09). Nevertheless, the outer sulfur atoms of DMET or EDTDM molecules have larger contribution to their HOMOs (atomic orbital coefficient ~0.15). Since the magnitude of the $\pi-d$ interaction is expected to be proportional to the square of atomic orbital coefficient at the intermolecular contact site, the $\pi-d$ interaction in the EDS–TTF salt becomes small compared to the DMET or EDTDM salt, in spite of the presence of considerable close contacts between donors and anions. It is also noteworthy that the intermolecular Br···Br distance between $FeBr_4$ anions is almost the same among the

EDS–TTF, DMET and EDTDM salts, whereas EDS–TTF salt shows no antiferromagnetic transition at least down to 1.8 K. The presence of the $\pi-d$ interaction in the DMET and EDTDM salts is therefore proved to be essential for the long-range magnetic ordering.

4. MOLECULAR CONDUCTING METAL BASED ON HALOGENATED DONORS

4.1. $(EDO–TTFBr_2)_2FeBr_4$

For the purpose of fabricating molecular conductors with good electrical condution, the molecular alignment should obviously be controlled so as to increase intermolecular overlap of the π-electron system. One of the strategies for this requirement is the introduction of the intermolecular interaction such as halogen$\cdots$halogen contacts. Closely connected halogen$\cdots$halogen contacts have geometrical preferences, whose origin is explained as the electrostatic forces anisotropy arising from the lone-pair electron density of the halogen atoms (26). From this viewpoint, this interaction has been utilized for the development of novel organic conductors based on halogenated TTF-derivatives (27).

Here we focus on the donor molecule EDO–TTFX_2 (X = Br, I) (28) as a constituent of molecular conducting magnets. Since the halogen substituents has high polarizability, the intermolecular halogen$\cdots$halogen interaction can serve not only as controlling the crystal structure, but also as a pathway for mediating magnetic interaction between the donor and magnetic anion. In addition, the TTF-derivatives having ethylenedioxy group(s) have strong tendency of giving stable metallic system (29), which is also a good character for obtaining molecular magnetic metals.

Figure 10 shows the crystal structure of (EDO–$TTFBr_2)_2FeBr_4$. In the crystal, the donor molecules are stacked in a head-to-tail fashion to form uniform 1D columns elongated along the c-axis. The tetrahedral $FeBr_4^-$ anions are located between the donor columns, forming 1D chains along the a-axis with intermolecular Br$\cdots$Br contacts (3.87 Å). The donor columns and anions are then linked with close intermolecular Br$\cdots$Br contacts, whose distance (3.54 Å) is significantly shorter than twice that of the van der Waals distance of the bromine atom ($2 \times 1.85 = 3.70$ Å) (17). These contacts play an important role in forming the uniform stacking of the donor molecules within the columns.

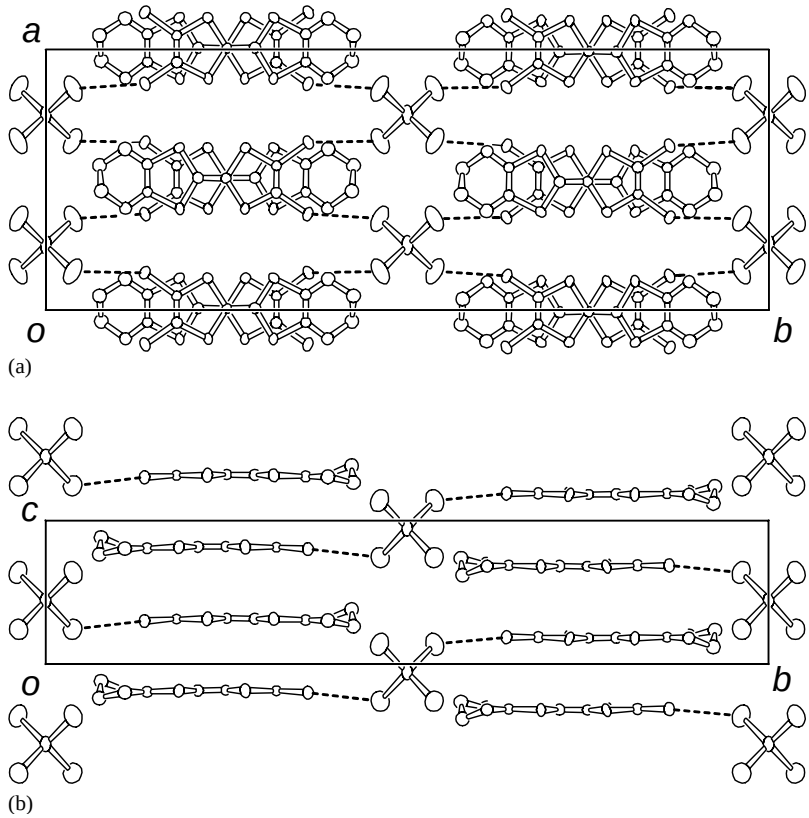

FIG. 10. Crystal structure of $(EDO–TTFBr_2)_2FeBr_4$ projected (a) along the c-axis and (b) a-axis. Dashed lines denote the intermolecular Br$\cdots$Br contacts between the donor and anion molecules.

This salt has high conductivity ($\sigma_{RT} = 200\,S\,cm^{-1}$) and shows metallic behavior. Around $T = 30\,K$, the resistivity takes a minimum, below which the salt shows semiconducting behavior. The magnetic susceptibility deviates from the Curie–Weiss law below $T \sim 200\,K$, suggesting the presence of strong antiferromagnetic interaction between the anion spins. Using the data of high-temperature region, the Weiss temperature is roughly estimated at $|\Theta| = 20$–$30\,K$. Below 40 K the magnetic anisotropy emerges, and at $T_N = 13.5\,K$ the susceptibility data show a kink when the field is applied parallel to the *a*-axis (Fig. 11). In this direction, the susceptibility takes a broad maximum around $T = 8\,K$ and then tends to vanish on the low-temperature side of the maximum. Although this complicated behavior cannot be explained as simple antiferromagnetism, the magnitude of T_N and $|\Theta|$ for this salt is the highest values among the $\pi-d$ interaction-based magnet thus far reported, suggesting the importance of Br···Br contacts between the donor and anion for the realization of magnetic interaction.

The origin of this strong intermolecular antiferromagnetic interaction can be explained by molecular orbital theory as follows. The semiempirical molecular orbital calculation using PM3 Hamiltonian (25) reveals that contribution of the Br 4*p* orbital to the HOMO of the EDO–$TTFBr_2$ molecule is negligibly small (atomic orbital coefficient = 0.06). However, this bromine contribution is considerably large for NHOMO (0.14) and LUMO (0.32), the latter of which has the σ-character and hence responsible for the intermolecular coordination. As a result, these molecular orbitals also can participate in the magnetic interaction through the close intermolecular Br···Br contacts between the π-electron system of the donor molecules and *d*-electron system of the magnetic anion, which leads to the large exchange interaction between the localized spins on the anions.

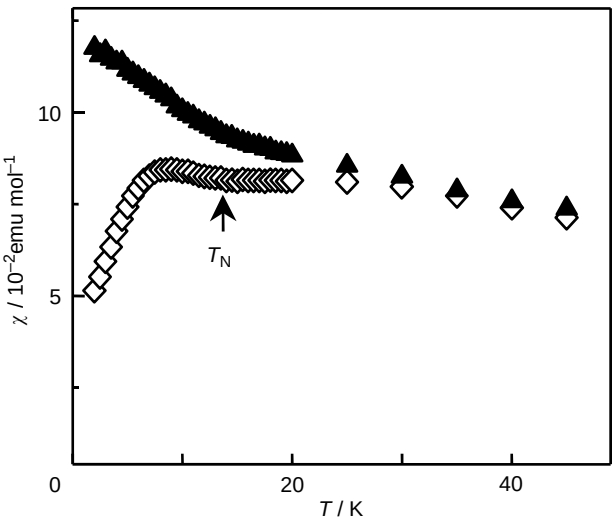

FIG. 11. Temperature dependence of the magnetic susceptibility of $(EDO–TTFBr_2)_2FeBr_4$ in a field of 1 T. Open diamonds: $B \parallel a$-axis, filled triangles: $B \parallel c$-axis.

4.2. $(EDO–TTFI_2)_2[M(mnt)_2]$ (M = Ni, Pt)

Molecular magnets based on $[M(mnt)_2]^-$ (M = Ni,Pt; *mnt* = maleonitriledithiolate) have been well studied (30), some of which show ferromagnetic interaction (31). We adopted these transition dithiolene complexes as a counterpart of the halogenated TTF-derivative from the following reasons (32): The unpaired *d*-electrons on the central metal atom are considerably delocalized to the ligands, which are experimentally confirmed by ESR spectra (33), hence the metal–dithiolene complexes can be a good candidates for achieving intermolecular magnetic interaction. This anion also contains cyano groups, which is expected to form strong –CN···I– coordination-bond-like interaction between the iodo group of the donor (27,34).

Figure 12 shows the crystal structure of (EDO–$TTFI_2)_2[M(mnt)_2]$ (M = Ni, Pt) (Fig. 1), which does not depend on the central atom of the counter anion. The donor and anion molecules form uniform 1D chains separately, both of which are elongated parallel to the *c*-axis. For the donor chain, the intermolecular transfer integrals between the donors are considerably large to form 1D π-electronic system. In the anion chain, on the other hand, the central metal atom of a complex molecule faces sulfur atoms of the adjacent molecules as featured with a slipped metal-over-sulfur configuration. Despite a short interplanar distance between the adjacent molecules (3.69 and 3.73 Å for M = Ni and Pt, respectively), the transfer integral between their SOMOs is negligibly small compared to the integrals within the donor chains. This "pseudo-orthogonal" configuration may arise from the presence of a strong intermolecular interaction between the iodo group of the donor and the CN group of the anion, whose distance (3.03 Å) is considerably smaller than the corresponding van der Waals distance (3.53 Å) (17). This closeness confirms the polarization of the $–CN^{\delta-}\cdots I^{\delta+}–$ interaction due to the positive charge on the donor molecule. Between the donor and anion columns short S···S contacts are also observed, whose distances are comparable to the van der Waals distance (3.70 Å).

These salts have high conductivities along the stacking direction of the molecules (110 and $170\,S\,cm^{-1}$ at room temperature for M = Ni and Pt, respectively) and show metallic behavior down to ca. 110 K. Below this temperature metal–insulator transitions take place, whose transition temperatures are estimated at 88 and 96 K for M = Ni and Pt, respectively, from the maximum of $d \ln \rho / d(T^{-1})$ vs T plots. In the low-temperature insulating state, the activation energies of the resistivity are considerably small,

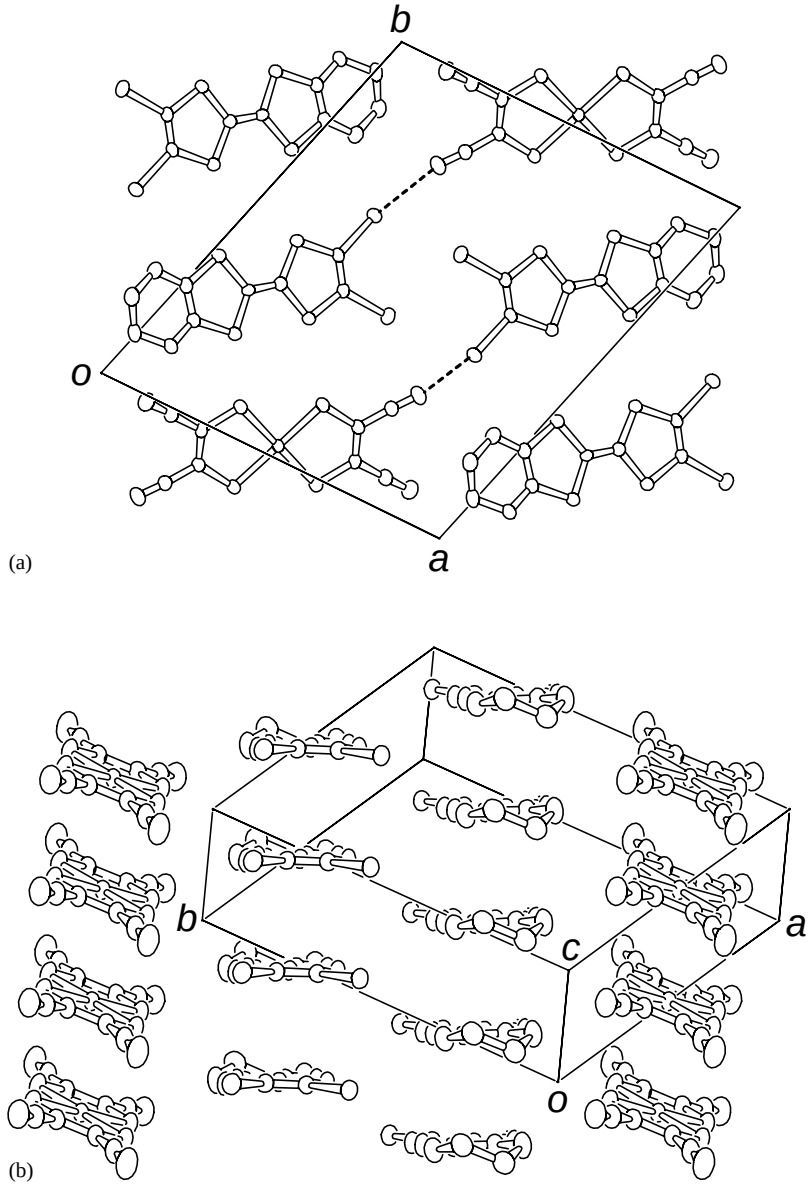

FIG. 12. Crystal structure of (EDO–$TTFI_2$)$_2$[M(mnt)$_2$] (M = Ni, Pt) projected (a) along the b-axis and (b) along the long axis of the donor molecules.

as estimated at $E_A = 60$ and 85 meV for M = Ni and Pt, respectively. Since no distinct change is detected on X-ray oscillation photographs from room temperature down to 16 K, their insulator phases can be ascribed to a $4k_F$ CDW or SDW state.

Figure 13(a) shows the temperature dependence of the magnetic susceptibility χ of (EDO-$TTFI_2$)$_2$[Ni(mnt)$_2$]. The value of χT at 300 K is estimated at 0.387 emu K mol^{-1}, which corresponds to one $S = 1/2$ spin per formula unit that is located on the [Ni(mnt)$_2$]$^-$ anion. As the temperature decreases, the χT value increases showing the presence of ferromagnetic interaction between the localized spins. The susceptibility χ is well fitted with the high-temperature expansion of the 1D $S = 1/2$ ferromagnetic Heisenberg model (Eq. (5)) using the Padé approximation (35)

$$\chi = \frac{N(g\mu_B)^2}{4k_B T} \left[\frac{1 + 5.7980K + 16.903K^2 + 29.377K^3 + 29.833K^4 + 14.037K^5}{1 + 2.7980K + 7.0087K^2 + 8.6539K^3 + 4.5743K^4}\right]^{2/3},$$

$$K = \frac{J}{4k_B T} \qquad [9]$$

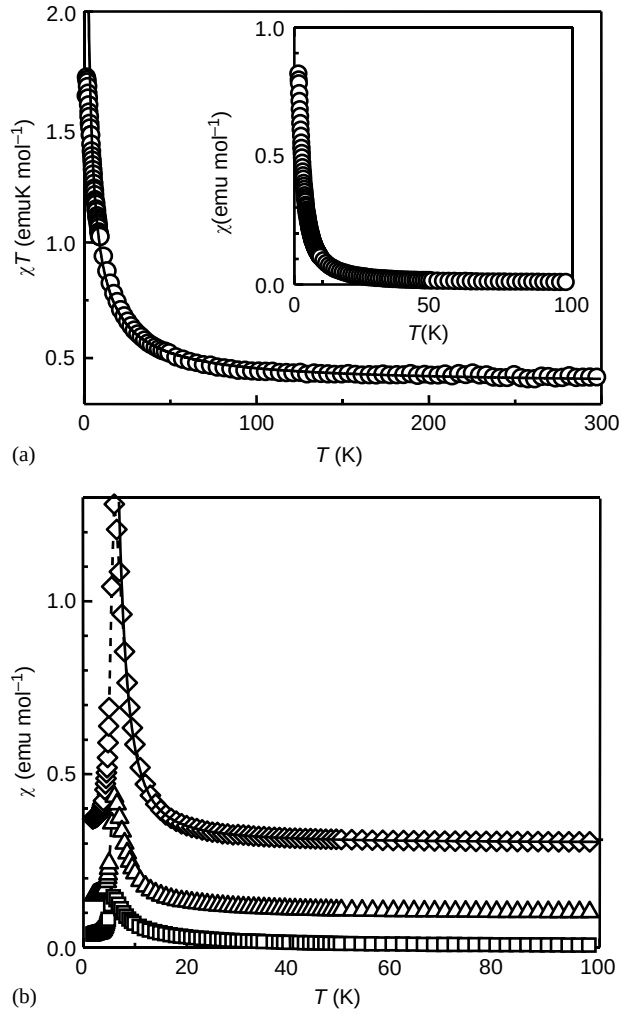

FIG. 13. (a) Temperature dependence of χT and χ (inset) for a single crystal of (EDO-TTFI$_2$)$_2$[Ni(mnt)$_2$] in a field of 0.1 T. The solid line is the theoretical curve for the $S=1/2$ 1D ferromagnet Heisenberg model ($J/k_B=36$ K). (b) Temperature dependence of the magnetic susceptibility for a single crystal of (EDO–TTFI$_2$)$_2$[Pt(mnt)$_2$] in a field of 10 mT. The solid line is the theoretical curve for the $S=1/2$ 1D ferromagnet Ising model ($J/k_B=40$ K). Squares: $B \parallel c$, diamonds: $B \parallel a-b$, triangles: $B \parallel a+b$. The data for $B \parallel a-b$ and $a+b$ axes are vertically shifted up by 0.3 and 0.1 emu mol^{-1}, respectively, for clarity. The dashed lines are guides for eyes.

with the exchange interaction $J/k_B=36$ K. No long-range magnetic ordering is detected down to 1.8 K, which is the consequence of the 1D Heisenberg magnet and suggests the weakness of the interchain interaction.

The replacement of the central atom of the anion to platinum causes different magnetic properties (Fig. 13(b)). The χT value 0.392 emu K mol^{-1} at 300 K is again consistent with an $S=1/2$ spin per anion. The susceptibility χ has a large anisotropy and well fitted with the exact solution of the susceptibility [11] of the 1D ferromagnetic Ising model [10] (36)

$$\hat{H} = -J \sum_i S_z^{(i)} S_z^{(i+1)}, \qquad [10]$$

$$\chi = \frac{N(g\mu_B)^2}{4k_B T} \exp(J/2k_B T), \qquad [11]$$

with the exchange interaction $J/k_B=40$ K, because of the large spin–orbit interaction of platinum atom. Furthermore, interchain antiferromagnetic interaction causes an antiferromagnetic transition at $T_N=5.5$ K. On the magnetization curve at $T=2$ K (Fig. 14(a)), an abrupt increase of the magnetization appears at $B_C=0.15$ T when the external field is applied parallel to the a–b axis. As the magnetization is already saturated just above the transition field B_C, this magnetic transition can be assigned as a metamagnet transition. From the transition field, the magnitude of the

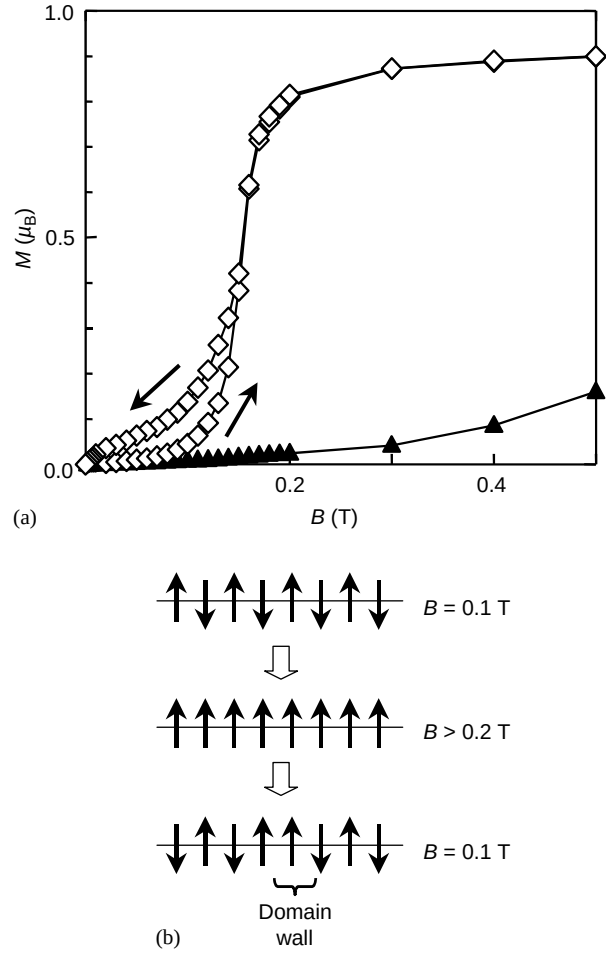

FIG. 14. (a) Magnetization curve of (EDO–TTFI$_2$)$_2$[Pt(mnt)$_2$] at 2 K, indicating the hysteretic behavior below $B=0.15$ T. The solid lines are guides for eyes. (b) Spin structure model for $B \parallel a-b$ axis. Arrows represent ferromagnetically ordered anion chains viewed along the c-axis.

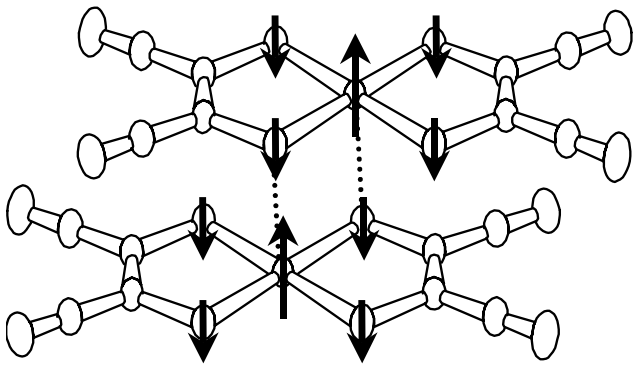

FIG. 15. Schematic representation of spin density of $M(mnt)_2$. Dotted line shows the "local" antiferromagnetic interaction.

interchain antiferromagnetic interaction is estimated at $J' = 50$ mK, which is comparable to the contribution of the dipole–dipole interaction. In addition to the metamagnetic transition, a hysteretic behavior appears in the low-field region just below B_C, which can be qualitatively explained with a model described in Fig. 14(b). In the field-increasing process below 0.1 T, ferromagnetically ordered chains are coupled antiferromagnetically. Then, above B_C, the spins in all the chains are parallelly aligned. In the field-decreasing process from B_C, many antiferromagnetic domains grow and domain walls appear at the boundaries. These "domain walls" are observed as the extra magnetization in the decreasing process.

The origin of the ferromagnetic interaction can be explained with McConnell's first model (37). In spite of the presence of short intermolecular atomic contacts between adjacent two $[M(mnt)_2]^-$ anions, the transfer integral between their SOMOs is negligibly small, which suppresses the antiferromagnetic coupling between their localized spins. The positive spin density on the central metal induces the negative spin on the sulfur atoms that are coordinated to the metal (38), which then couples with the positive spin on the central metal of adjacent molecules through "local" antiferromagnetic interaction (Fig. 15). As a result, the spins on the central metal are ferromagnetically aligned in the anion column.

5. CONCLUSION

We have developed conducting molecular magnets based on TTF-type donors and magnetic counter anions, which are classified into two groups in the present article. The first part involves $(DMET)_2FeBr_4$ and related salts. $(DMET)_2FeBr_4$ shows metallic behavior down to ca. 40 K, where the SDW transition takes place. The magnetic anions undergo an antiferromagnetic ordering, whose three dimensionality shows the presence of magnetic interaction through the donor layer. The magnetization curves in the antiferromagnetic phase show complex behavior, suggesting the contribution of the localized π-electrons on the donor layers. The interplay of the π-electrons on the donor side and the d-electrons on the anion side is directly proven by the coincidence of the anomalies on the magnetoresistance and magnetization curves. The results on the related salts support this conclusion. $(EDTDM)_2FeBr_4$ elucidates the role of π-electrons in the physical properties, whereas the lack of the $\pi-d$ interaction in $(EDS–TTF)_2FeBr_4$ indicates the importance of the intermolecular overlap for the establishment of the $\pi-d$ interaction.

In the second part, we presented the molecular conducting magnet with a halogenated TTF-derivatives. The crystal structures of $(EDO–TTFBr_2)_2FeBr_4$ and $(EDO–TTFI_2)_2[M(mnt)_2]$ (M = Ni, Pt) are characterized as the presence of strong intermolecular Br$\cdots$or I$\cdots$NC bonds, respectively. In the former salt the antiferromagnetic interaction between the magnetic anion is quite large, presumably due to the presence of this intermolecular contact. In the latter salts, the magnetic anions are stacked so that McConnel's first model is applicable, leading to the coexistence of metallic conduction and ferromagnetic interaction first observed in the molecular conducting magnets.

As mentioned above, organic complex-based molecular magnets based on TTF-type donor molecules and magnetic counter anions are found to be good targets for the development of molecular magnetism. The most important feature of these materials is the interplay of electrical transport and magnetic properties. When the π-electronic system on the donor molecules is in the marginal region between metal and insulator phases, magnetic ordering of the anion layer strongly affects the transport properties on the donor layer. This will lead to the appearance of magnetotransport properties such as a giant magnetoresistance, which is drawing attention also from the viewpoints of application. On the other side, if the metallic π-electronic system is sufficiently stabilized, the localized d-electrons will interact each other via free-electron-like conduction carriers to produce long-range interaction known as the Ruderman–Kittel–Kasuya–Yoshida (RKKY) interaction (39). Since this interaction is the origin of strong magnetism emerging in rare-earth magnetic metals for example, the stabilization of metallic π-electronic system will cause an evolution from conducting molecular magnets into molecular magnetic metals. In addition, since the RKKY exchange interaction has a spatially oscillatory behavior between ferromagnetic and antiferromagnetic nature depending on the Fermi wave number k_F of the conduction electron system, a suitable design of π-electronic conduction layer and d-electronic magnetic layer will produce molecular ferromagnetic metal magnets,

which is regarded as one of the challenging targets of molecular magnets.

ACKNOWLEDGMENTS

This work was supported by a Grant-in-Aid for Scientific Research on Priority Area (No. 12046231) from the Ministry of Education, Science, Sports, and Culture, Japan.

REFERENCES

1. (a) J. M. Williams, J. R. Ferraro, R. J. Thorn, K. D. Carlson, U. Geiser, H.-H. Wang, A. M. Kini, and M.-H. Whangbo, *in* "Organic Superconductors. Synthesis, Structure, Properties and Theory" (R. N. Grimes, Ed.). Prentice–Hall, Englewood Cliffs, NJ, 1992; (b) T. Ishiguro, K. Yamaji, and G. Saito, "Organic Superconductors," Springer-Verlag, Heidelberg, Germany, 1998.
2. "Proceedings of International Conference on Science and Technology of Synthetic Metals." *Synth. Met.* **101–103** (1999), **119–121** (2001).
3. J. Ferrais, D. O. Cowan, V. Walatka Jr., and J. H. Perlstein, *J. Am. Chem. Soc.* **95,** 948 (1973).
4. G. Grüner, "Density Waves in Solids," Frontiers in Physics, Addison–Wesley, Reading, MA, 1994.
5. (a) S. Tomonaga, *Prog. Theor. Phys.* **5,** 544 (1950); (b) J. M. Luttinger, *J. Math. Phys.* **4,** 1154 (1963).
6. M. Tamura, Y. Nakazawa, D. Shioi, K. Nozawa, Y. Hosokoshi, M. Ishikawa, M. Takahashi, and M. Kinoshita, *Chem. Phys. Lett.* **186,** 401 (1991).
7. J. S. Miller, J. C. Calabrese, H. Rommelmann, S. R. Chittipeddi, J. H. Zhang, W. M. Reiff, and A. J. Epstein, *J. Am. Chem. Soc.* **109,** 769 (1987).
8. (a) T. Enoki, J. Yamaura, and A. Miyazaki, *Bull. Chem. Soc. Jpn.* **70,** 2005 (1997); (b) A. Miyazaki, M. Enomoto, M. Enomoto, T. Enoki, and G. Saito, *Mol. Cryst. Liq. Cryst.* **305,** 425 (1997); (c)T. Enoki, T. Umeyama, M. Enomoto, J. Yamaura, K. Yamaguchi, A. Miyazaki, E. Ogura, Y. Kuwatani, M. Iyoda, and K. Kikuchi, *Synth. Met.* **103,** 2275 (1999); (d) A. Miyazaki, T. Umeyama, T. Enoki, E. Ogura, Y. Kuwatani, M. Iyoda, H. Nishikawa, I. Ikemoto, and K. Kikuchi, *Mol. Cryst. Liq. Cryst.* **334,** 379 (1999); (e) A. Miyazaki, M. Enomoto, K. Enomoto, J. Nishijo, T. Enoki, E. Ogura, Y. Kuwatani, and M. Iyoda, *Mol. Cryst. Liq. Cryst.* **376,** 535 (2002).
9. (a) J. Yamaura, K. Suzuki, Y. Kaizu, T. Enoki, K. Murata, and G. Saito, *J. Phys. Soc. Jpn.* **65,** 2645 (1996); (b) M. Watabnabe, Y. Nogami, K. Oshima, J. Yamaura, T. Enoki, and G. Saito, *Solid State Commun.* **100,** 755 (1996); (c) R. Tsuchiya, S. Yoshizaki, T. Nakamura, T. Takahashi, J. Yamaura, K. Suzuki, T. Enoki, and G. Saito, *Synth. Met.* **70,** 967 (1995).
10. (a) M. Enomoto, A. Miyazaki, and T. Enoki, *Mol. Cryst. Liq. Cryst.* **335,** 293 (1999); (b) M. Enomoto, A. Miyazaki, and T. Enoki, *Bull. Chem. Soc. Jpn.* **74,** 459 (2001); (c) M. Enomoto, A. Miyazaki, T. Enoki, *Synth. Met.* **121,** 1800 (2001).
11. (a) T. Kominami, T. Matsumoto, K. Ueda, T. Sugimoto, K. Murata, M. Shiro, and H. Fujita, *J. Mater. Chem.* **11,** 2089 (2001); (b) T. Naito, T. Inabe, K. Takeda, K. Awaga, T. Akutagawa, T. Hasegawa, T. Nakamura, T. Kakiuchi, H. Sawa, T. Yamamoto, and H. Tajima, *J. Mater. Chem.* **11,** 2221 (2001); (c) L. Ouahab, *Chem. Mater.* **9,** 109 (1997); (d) E. Coronado, J. R. Galán-Mascarós, C. J. Gómez-García, and V. Laukhin, *Nature* **408,** 447 (2000).
12. (a) A. Kobayashi, T. Udagawa, H. Tomita, T. Naito, and H. Kobayashi, *Chem. Lett.* 2179 (1993); (b) H. Kobayashi, H. Tomita, T. Naito, A. Kobayashi, F. Sakai, T. Watanabe, and P. Cassoux, *J. Am. Chem. Soc.* **118,** 368 (1996); (c) H. Kobayashi, A. Kobayashi, and P. Cassoux, *Chem. Soc. Rev.* **29,** 325 (2000).
13. S. Uji, H. Shinagawa, T. Terashima, T. Yakabe, Y. Terai, M. Tokumoto, A. Kobayashi, H. Tanaka, and H. Kobayashi, *Nature* **410,** 908 (2001).
14. K. Bechgaard, C. S. Jacobsen, K. Mortensen, J. H. Pedersen, and N. Thorup, *Solid State Commun.* **33,** 1119 (1980).
15. (a) T. Mori, *Bull. Chem. Soc. Jpn.* **71,** 2509 (1998); (b) T. Mori, H. Mori, and S. Tanaka, *Bull. Chem. Soc. Jpn.* **72,** 179 (1999).
16. (a) I. Ikemoto, K. Kikuchi, K. Saito, K. Kanoda, T. Takahashi, K. Murata, and K. Kobayashi, *Mol. Cryst. Liq. Cryst.* **181,** 185 (1990); (b) K. Murata, K. Kikuchi, T. Takahashi, K. Kobayashi, Y. Honda, K. Saito, K. Kanoda. T. Tokiwa, H. Anzai, and T. Ishiguro, *J. Mol. Elect.* **4,** 173 (1988).
17. A. Bondi, *J. Phys. Chem.* **68,** 441 (1964).
18. (a) K. Kanoda, T. Takahashi, K. Kikuchi, K. Saito, I. Ikemoto, and K. Kobayashi, *Synth. Met.* **27,** *B* 269 (1988); (b) H. Yoshino, K. Saito, T. Sato, H. Nishikawa, K. Kikuchi, K. Kobayashi, and I. Ikemoto, *Synth. Metals* **96,** 19 (1998).
19. K. Enomoto, A. Miyazaki, and T. Enoki, *Synth. Met.* **120,** 977 (2001).
20. Y. Ishikawa, K. Saito, K. Kikuchi, K. Kobayashi, and I. Ikemoto, *Bull. Chem. Soc. Jpn.* **64,** 212 (1991).
21. T. Mori, A. Kobayashi, Y. Sasaki, H. Kobayashi, G. Saito, and H. Inokuchi, *Bull. Chem. Soc. Jpn.* **57,** 627 (1984).
22. (a) A. Kobayashi, H. Kim, Y. Sasaki, R. Kato, H. Kobayashi, S. Moriyama, Y. Nishio, K. Kajita, and W. Sasaki, *Chem. Lett.* 1819 (1987); (b) A. Kobayashi, H. Kobayashi, A. Miyamoto, R. Kato, R. A. Clark, and A. E. Underhill, *Chem. Lett.* 2163 (1991).
23. H. Yoshino, K. Saito, K. Kikuchi, I. Ikemoto, and K. Kobayashi, *Synth. Met.* **72,** 141 (1995).
24. K. Okabe, K. Enomoto, A. Miyazaki, and T. Enoki, *Mol. Cryst. Liq. Cryst.* **376,** 513 (2002).
25. J. J. P. Stewart, *J. Comp. Chem.* **10,** 209 (1989).
26. S. L. Price, A. J. Stone, J. Lucas, R. S. Rowland, and A. E. Thornle, *J. Am. Chem. Soc.* **116,** 4910 (1994).
27. (a) T. Imakubo, H. Sawa, and R. Kato, *J. Chem. Soc. Chem. Commun.* 1097, 1667 (1995); (b) M. Iyoda, H. Suzuki, S. Sasaki, H. Yoshino, K. Kikuchi, K. Saito, I. Ikemoto, H. Matsuyama, and T. Mori, *J. Mater. Chem.* **6,** 501 (1996); (c) B. Domercq, T. Devic, M. Fourmigué, P. Auban-Senzier, and E. Canadell, *J. Mater. Chem.* **11,** 1570 (2001).
28. M. Iyoda, Y. Kuwatani, E. Ogura, K. Hara, H. Suzuki, T. Takano, K. Takeda, J. Takano, K. Ugawa, M. Yoshida, H. Matsuyama, H. Nishikawa, I. Ikemoto, T. Kato, N. Yoneyama, J. Nishijo, A. Miyazaki, and T. Enoki, *Heterocycles* **54,** 833 (2001).
29. S. Horiuchi, H. Yamochi, G. Saito, K. Sakaguchi, and M. Kusunoki, *J. Am. Chem. Soc.* **118,** 8604 (1996).
30. (a) P. I. Clemenson, *Coord. Chem. Rev.* **106,** 171 (1990); (b) M. B. Hursthouse, R. L. Short, P. I. Clemenson, and A. E. Underhill, *J. Chem. Soc. Dalton Trans.* 1101 (1989); (c) M. B. Hursthouse, R. L. Short, P. I. Clemenson, and A. E. Underhill, *J. Chem. Soc. Dalton Trans.* 1101 (1989); (d) V. Gama, R. T. Henriques, G. Bonfait, M. Almeida, A. Meetsma, S. van Smaalen, and J. L. De Boer, *J. Am. Chem. Soc.* **114,** 1986 (1992); (e) V. Gama, R. T. Henriques, G. Bonfait, L. C. Pereira, J. C. Waerenborgh, I. C. Santos, M. T. Duarte, J. M. P. Cabral, and M. Almeida, *Inorg. Chem.* **31,** 2598 (1992); (f) W. Reith, K. Polborn, and E. Amberger, *Angew. Chem. Int. Ed. Engl.* **27,** 699 (1988).
31. (a) M. Uruichi, K. Yakushi, Y. Yamashita, and J. Qin, *J. Mater. Chem.* **8,** 141 (1998); (b) M.L. Allan, A. T. Coombar, I. R. Marsden, A. Charlton, and A. E. Underhill, *Synth. Met.* **55–57,** 3317 (1993);

J. S. Miller, J. C. Calabress, and A. J. Epstein, *Inorg. Chem.* **28,** 4230 (1989).
32. J. Nishijo, A. Miyazaki, T. Enoki, E. Ogura, T. Takano, Y. Kuwatani, M. Iyoda, and J. Yamaura, *Solid State Commun.* **116,** 661–664 (2000).
33. R. Kirmse, J. Stach, W. Dietsch, G. Steimecke, and E. Hoyer, *Inorg. Chem.* **19,** 2679 (1980).
34. (a) G. R. Desiraju and R. L. Harlow, *J. Am. Chem. Soc.* **111,** 6757 (1989); (b) J. P. M. Lommerse, A. J. Stone, R. Taylor, and F. H. Allen, *J. Am. Chem. Soc.* **118,** 3108 (1996).
35. G. Ch. Baker, G. S. Rushbrooke, and H. E. Gilbert, *Phys. Rev.* **135,** A1272 (1964).
36. E. Ising, *Z. Physik.* **31,** 253 (1925).
37. H. M. McConnell, *J. Chem. Phys.* **39,** 1910 (1963).
38. A. T. Coomber, D. Beljonne, R. H. Friend, J. L. Brédas, A. Charlton, N. Robertson, A. E. Underhill, M. Kurmoo, and P. Day, *Nature* **380,** 144 (1996).
39. (a) M. A. Ruderman and C. Kittel, *Phys. Rev.* **96,** 99 (1954); (b) T. Kasuya, *Prog. Theor. Phys.* **16,** 45 and 58 (1956); (c) K. Yoshida, *Phys. Rev.* **106,** 893 (1957).